

Combining electron microscopy with atomic-scale calculations—A personal perspective

Sokrates T. Pantelides

Citation: Chin. Phys. B, 2024, 33 (**12**): 120704. DOI: 10.1088/1674-1056/ad8ece
Journal homepage: http://cpb.iphy.ac.cn; http://iopscience.iop.org/cpb

What follows is a list of articles you may be interested in

Capturing the non-equilibrium state in light—matter—free-electron interactions through ultrafast transmission electron microscopy

Wentao Wang(汪文韬), Shuaishuai Sun(孙帅帅), Jun Li(李俊), Dingguo Zheng(郑丁国), Siyuan Huang(黄思远), Huanfang Tian(田焕芳), Huaixin Yang(杨槐馨), and Jianqi Li(李建奇)
Chin. Phys. B, 2024, 33 (**1**): 010701. DOI: 10.1088/1674-1056/ad0141

Loading uniform Ag_3PO_4 nanoparticles on three-dimensional peony-like WO_3 for good stability and excellent selectivity towards NH_3 at room temperature

Xingyan Shao(邵星炎), Fuchao Jia(贾福超), Tingting Liu(刘婷婷), Jiancheng Liu(刘健诚), Xiaomei Wang(王小梅), Guangchao Yin(尹广超), Na Lv(吕娜), Tong Zhou(周通), Ramachandran Rajan, and Bo Liu(刘波)
Chin. Phys. B, 2023, 32 (**8**): 080703. DOI: 10.1088/1674-1056/ac98a0

Construction of multi-walled carbon nanotubes/$ZnSnO_3$ heterostructures for enhanced acetone sensing performance

Liyong Du(杜丽勇) and Heming Sun(孙鹤鸣)
Chin. Phys. B, 2023, 32 (**5**): 050701. DOI: 10.1088/1674-1056/ac89da

Copper ion beam emission in solid electrolyte $Rb_4Cu_{16}I_{6.5}Cl_{13.5}$

Tushagu Abudouwufu(吐沙姑·阿不都吾甫), Xiangyu Zhang (张翔宇), Wenbin Zuo (左文彬), Jinbao Luo(罗进宝), Yueqiang Lan(兰越强), Canxin Tian (田灿鑫), Changwei Zou(邹长伟), Alexander Tolstoguzov, and Dejun Fu(付德君)
Chin. Phys. B, 2022, 31 (**4**): 040704. DOI: 10.1088/1674-1056/ac2f31

In-situ fabrication of ZnO nanoparticles sensors based on gas-sensing electrode for ppb-level H_2S detection at room temperature

Jing-Yue Xuan(宣景悦), Guo-Dong Zhao(赵国栋), Xiao-Bo Shi(史小波), Wei Geng(耿伟), Heng-Zheng Li(李恒征), Mei-Ling Sun(孙美玲), Fu-Chao Jia(贾福超), Shu-Gang Tan(谭树刚), Guang-Chao Yin(尹广超), and Bo Liu(刘波)
Chin. Phys. B, 2021, 30 (**2**): 020701. DOI: 10.1088/1674-1056/abcf46

TOPICAL REVIEW — Stephen J. Pennycook: A research life in atomic-resolution STEM and EELS

Combining electron microscopy with atomic-scale calculations — A personal perspective

Sokrates T. Pantelides[†]

Department of Physics and Astronomy and Department of Electrical and Computer Engineering, Vanderbilt University, Nashville, Tennessee 37235, USA

(Received 14 October 2024; revised manuscript received 14 October 2024; accepted manuscript online 5 November 2024)

I had the privilege and the pleasure to work closely with Stephen J. Pennycook for about twenty years, having a group of post-docs and Vanderbilt-University graduate students embedded in his electron microscopy group at Oak Ridge National Laboratory, spending on average a day per week there. We combined atomic-resolution imaging of materials, electron-energy-loss spectroscopy, and density-functional-theory calculations to explore and elucidate diverse materials phenomena, often resolving long-standing issues. This paper is a personal perspective of that journey, highlighting a few examples to illustrate the power of combining theory and microscopy and closing with an assessment of future prospects.

Keywords: electron microscopy, EELS, density-functional-theory calculations

PACS: 07.78.+s, 61.72.Bb, 61.46.Hk **DOI:** 10.1088/1674-1056/ad8ece

1. Introduction

This perspective is a tribute to Stephen J. Pennycook, a pioneer and innovator in scanning transmission electron microscopy (STEM) and STEM-based electron-energy-loss spectroscopy (EELS). I am one of the original practitioners of density-functional-theory (DFT) calculations, which emerged as the quantum tool of choice to compute properties of materials in the 1970's. After 20 years at the IBM T. J. Watson Research Center in New York, I joined the faculty at Vanderbilt University in the fall of 1994. Gerry Mahan invited me to ORNL to give a talk and by the end of the day I was offered a secondary appointment to start a group, initially with a single post-doc, spending a day per week or so, embedded in Steve Pennycook's group. I accepted and the rest is history.

Atomic-resolution electron microscopy, EELS, and DFT calculations are incredibly complementary techniques that can jointly address issues and puzzles in materials, nanostructures that emerged as "nanoscience" in the late 1990's, and the juggernaut of two-dimensional materials in the 2000's. STEM-based Z-contrast imaging depicts columns of atoms or individual atoms with an intensity that depends strongly on the net atomic number Z, while a primary strength of DFT calculations is to determine the energetically preferred atomic configurations. EELS at the time explored primarily electronic transitions from core levels to available final states. The pertinent final states are not empty conduction-band states because the core hole left behind is so localized near the nucleus that it behaves like an extra proton on that nucleus; as a result, the density of empty states that is calculated by replacing the host atom of atomic number Z with a $Z+1$ atom features the same sequence of peaks as those of EELS in a suitable energy range above the threshold or "edge". Absolute edge energies could not be calculated with sufficient energy so a positioning of the theoretical spectrum on the energy axis to match the first theoretical peak with the first EELS peak was necessary. On the other hand, the EELS edges (K-edge for 1s core levels, $L_{2,3}$ edge for the spin–orbit split 2p core levels, M edges for the spin–orbit split 3d levels, and so on) are clear signatures of each element so that, once atomic-resolution became possible, chemical maps became possible complementing the more precise Z-contrast structural maps

Steve and I, staff microscopists, and a constant stream of post-docs, graduate students, and visiting scientists from around the world worked closely together for ~ 20 years until Steve left ORNL. The theory presence in the group grew substantially over those years. We have published a total of 131 co-authored papers, most of them in high-profile journals, that have by now accumulated more than 9500 citations (73 citations per paper) and an H-index of 55 by themselves (Web of Science data). All of this productivity was the result of an amazing group that Steve assembled at ORNL over the years, which included a literally uncountable stream of visiting scientists from the US, Europe, and Asia, many of whom were funded by their own institutions to visit and work with Steve. I had the pleasure and privilege to interact and co-author papers with many of them. My days at ORNL were truly exhilarating, and often very long, making the rounds with Steve to review ongoing projects and discussing new experimental data. I would occasionally stay a second night during which many of us would hang out at a restaurant and enjoy libations.

One component that enriched my experiences at ORNL was the fact that several of my graduate students at Vanderbilt

[†]Corresponding author. E-mail: pantelides@vanderbilt.edu

© 2024 Chinese Physical Society and IOP Publishing Ltd

opted to do a joint theory and microscopy thesis. They would finish their coursework and get trained on theory at Vanderbilt and then move to ORNL where they got direct mentorship from staff group members and Steve.

As Steve once told me, "a picture may be worth a thousand words, but a picture is still just a picture unless there is a story to tell — that's where theory comes in". This short perspective aims to give my personal account of just a few of the "stories" that we built by combining "pictures" and "theory", a personal perspective of the power of combining microscopy and theory. These stories illustrate the twists and turns of figuring things out, pushing then-current computer capabilities, and also some of the frustrations arising from an inability to follow-up to test predictions when theory went beyond the data at hand. In what follows, only our original papers are cited, wherein one can find citations to other works.

2. Impurity segregation in grain boundaries

This project brings back fond memories because it was our very first joint work that started in 1995 and led to an assortment of intriguing results. We started with a question that was generated in the arena of Si-based electronics. In those days, the gate metal in metal–oxide–semiconductor field-effect transistors (MOSFETs) was heavily doped polycrystalline Si. It was known that a large fraction of arsenic impurities segregate in the grain boundaries (GBs) and do not behave as dopants. The segregation energy (energy difference between an As atom substituting a Si atom in the grain and in the GB) was measured to range from 0.41 eV to 0.65 eV. It would, therefore, be useful to know if the phenomenon is intrinsic and unavoidable or it is caused by poor-quality, defect-containing GBs. It was also known that tilt GBs in undoped Si rebond so that all atoms are fourfold coordinated as in the bulk crystal. Prior calculations indeed found that, for such grain boundaries, the segregation energy is only ~ 0.1 eV, leading to the inference that defects must be present for stronger bonding by As atoms in tilt GBs.

While imaging of an As-doped Si tilt GB was pursued diligently by staff microscopist Matt Chisholm, calculations by our first post-doc, Amitesh Maiti, actually went fast, motivated by my prior experience with amorphous silicon: Arsenic is not a very efficient dopant in amorphous Si because in most environments it manages to achieve threefold-coordinated bonding, which is energetically preferred (formation of three strong bonds, while the remaining two electrons go lower in energy as "lone pairs", i.e., a non-doping configuration). We, therefore, examined how As might achieve threefold-coordinated bonding in a defect-free tilt Si GB that we shall call GB1. We found that two neighboring substitutional As atoms in select columns lower their energy by repelling each other, which results in them achieving stable threefold coordination (Fig. 1(a)) with a segregation energy of 0.2 eV. Larger segregation energies (0.3–0.5 eV per As atom) can be achieved by the formation of chains of such As dimers, i.e., fully ordered chains of threefold-coordinated As atoms.[1] Imaging of such chains came soon after.[2] Figure 1(b) shows the calculated charge density around such chains and Fig. 1(c) shows Z-contrast images of such chains and a schematic of the image. Problem solved!

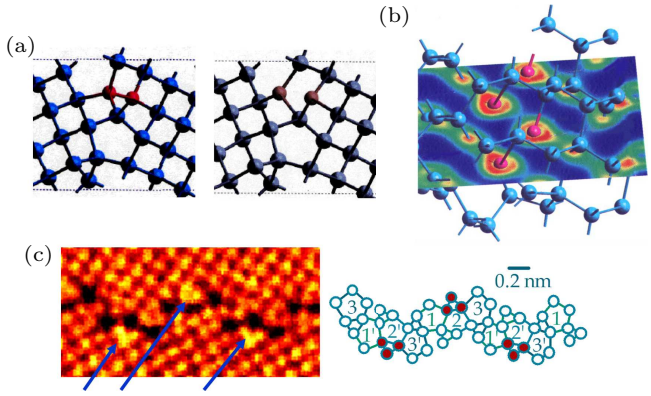


Fig. 1. Arsenic segregation in Si tilt grain boundaries. (a) Schematics illustrating how two substitutional As impurities in the GB can stabilize in threefold coordination by repelling each other. (b) Electron density in a plane cutting across As chains in a GB. (c) Z-contrast image of a Si tilt GB doped with As. Arrows point to the winding chains of threefold-coordinated As chains, confirming the theoretical prediction.

Theory went one step further, however. We tested different tilt GBs and found that formation of such threefold-coordinated As atoms could in some cases induce a structural transformation of the GB. More specifically, we found an alternative structure of the same GB, call it GB2, whose energy is only slightly higher than that of GB1. Upon doping both with As, we found that GB2 has lower energy. The group at ORNL, however, did not have the expertise to follow up with experiments to demonstrate the realization of an impurity-induced GB structural transformation.

The inability to follow up on ideas that arise from resolving a puzzle can indeed be frustrating, but in the case of an impurity-induced GB structural transformation, we got very lucky. Yanfa Yan, a post-doc in microscopy who actually volunteered and learned how to perform DFT calculations, had just obtained a Z-contrast image of a MgO bicrystal that was procured with the understanding that it had undetectable impurity concentrations. The structure extracted from the Z-contrast image of the GB did not match the accepted structure of that particular tilt GB (Fig. 2). The image, however, had some Mg columns that were easily recognized to be brighter than the others, designated by arrows in the Z-contrast image of Fig. 2, signaling that an impurity heavier than Mg must be lurking in there. EELS was brought into action and quickly found a Ca edge only when the electron beam was placed on those brighter columns. So what? It was theory's turn. Calculations of the total energy per Mg–O pair in the two GBs

without impurities verified that the previously accepted structure was indeed energetically preferred. When Ca impurities were inserted to replace Mg atoms in the two different GBs, however, the newly determined structure had the lower energy — proof that we witnessed an impurity-induced GB structural transformation! The paper was published in 1998.[3]

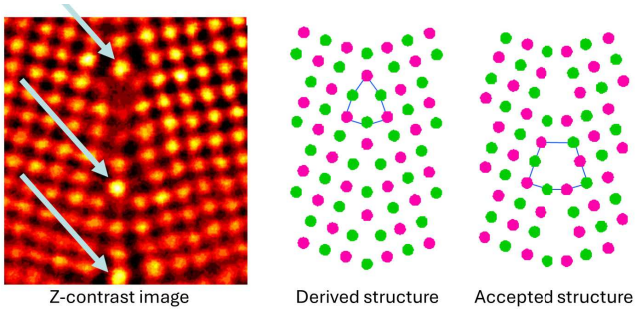


Fig. 2. Ca-doped tilt GB in MgO. Arrows indicate columns containing Ca impurities, as identified by core-loss EELS. The "derived structure" differs from the "accepted structure" of the pristine form of this GB. Theory demonstrated that the derived structure is the result of an impurity-induced structural transformation of the GB.

The saga of impurities in GBs continued in 2005, spearheaded by Robert Klie in a broad collaboration.[4] This time it was GBs in the high-temperature superconductor $YBa_2Cu_3O_{7-\delta}$ (YBCO), which posed a long-standing puzzle. Grain boundaries were known to reduce the superconducting critical current density J_c of YBCO and polycrystalline material was the only practical option for large-scale applications. It was found, however, that adding Ca impurities to YBCO leads to increased J_c. The effect was generally attributed to excess holes introduced by divalent Ca substituting trivalent Y, which left out any role of the GBs. Robert had *Z*-contrast images and atomic-resolution EELS, but their interpretation was challenging. DFT calculations in this case faced a seemingly insurmountable difficulty — there was no way that computers available at the time could handle periodic supercells large enough to fit the necessary two oppositely oriented GBs in the very complex YBCO structure. We were, in fact, able to resolve the Ca puzzle without doing a single GB calculation.

Here is how it worked out. It was already known that Ca segregates in YBCO GBs and it was believed that it substitutes Y there as well. It was also known, however that large strains, of order as high as 10%, both compressive and tensile, occur at the dislocation cores that comprise the GBs. We performed DFT calculations in bulk crystalline YBCO under both compression and tension. As shown in Fig. 3(a), we found that, in unstrained YBCO, it is indeed energetically preferred for Ca to substitute Y. In regions under compressive strain, however, substitution for Ba is increasingly possible and becomes energetically favorable at strains greater than $\sim 6\%$. Similarly, in regions under tensile strain, substitution for Cu becomes favorable.

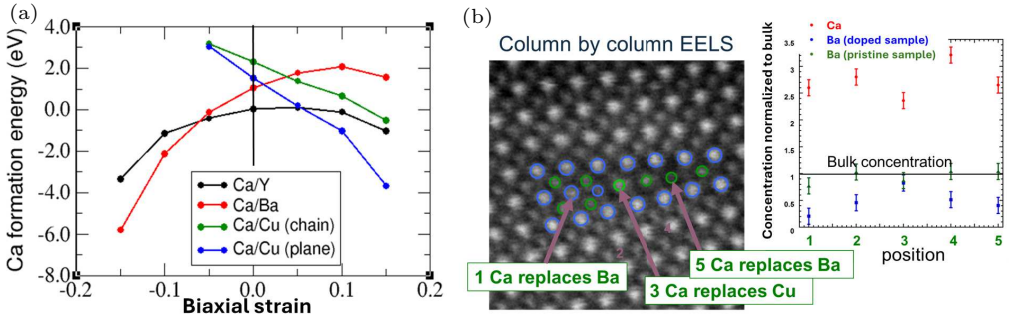


Fig. 3. Calcium impurities in YBCO GBs. (a) Ca formation energies substituting Y, Ba, or Cu in biaxially strained crystalline YBCO lead to predictions of the preferred substitutional sites in a GB that has regions of compressive and tensile strain. (b) Column-by-column EELS confirms predictions.

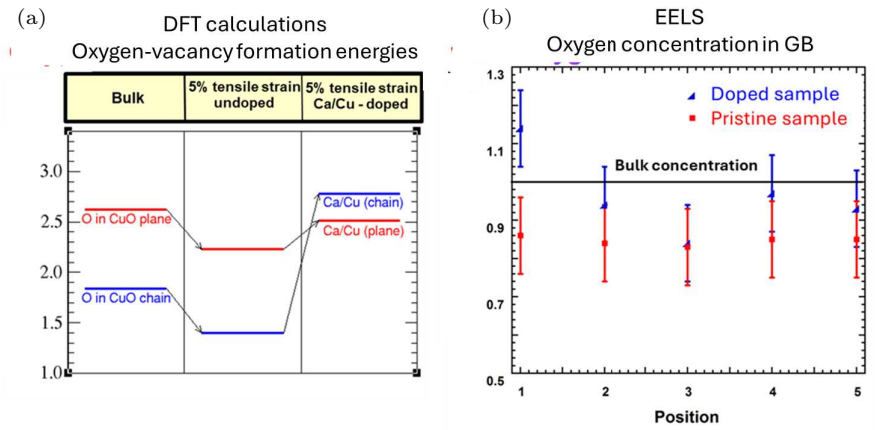


Fig. 4. (a) Calculated oxygen-vacancy formation energies in bulk YBCO and (b) EELS-derived oxygen concentrations in Ca-doped and pristine YBCO GBs are consistent and help unveil the role of Ca doping in raising the YBCO critical current density.

In contrast, strain has only a small effect on substitution for Y. Column-by-column EELS, shown in Figs. 3(b) and 3(c) are fully consistent with these theoretical predictions. Clearly, the relative ionic sizes drive the defect formation energies: the ionic radii of Ca and Y are roughly equal, but the radius of Cu is $\sim$ 30% smaller and the radius of Ba is $\sim$ 30% larger. The chemical valence of impurities becomes secondary in the presence of these high strains. The net inference is that Ca substitution at GBs occurs in order to reduce the local strain.

DFT calculations further found, that in strained, undoped YBCO, the formation energies for O vacancies are significantly reduced relative to those in unstrained-bulk values, whereas in Ca-doped YBCO, O-vacancy formation energies in strained YBCO increase relative to those in Ca-doped unstrained bulk (Fig. 4(a)). Oxygen concentrations in GBs extracted from column-by-column EELS (Fig. 4(b)) are consistent with these predictions. The inference is that Ca-doping reduces significantly the concentration of O vacancies in Ca-doped GBs, which then exhibit reduced hole depletion. The final inference is that excess O vacancies in undoped YBCO GBs are responsible for the observed reduction in J_c in polycrystalline YBCO, while the role of Ca is to remove the intrinsic excess of O vacancies from the GBs. Thus, high critical currents are restored through a cooperative doping mechanism.

3. Complex oxides

We did a large number of projects on diverse oxides, such as MgO and YBCO discussed above, the family of aluminas (Al_2O_3), and especially oxides in the perovskite structure, including perovskite-oxide heterostructures and superlattices, for which microscopy was largely driven by group microscopists Albina Borisevich or Maria Varela. I will mention just two projects in which we resolved long-standing issues. The first, in which electron microscopy was driven by Albina,[5] was about Al_2O_3, which comes in several polymorphs, on which we wrote quite a few papers. Porous γ-Al_2O_3, a widely used catalyst and catalytic support, transforms to non-porous α-Al_2O_3 at $\sim$ 1100 °C, but refinery applications require stability at even higher temperatures. The problem had been solved by the discovery that doping γ-Al_2O_3 with lanthanum raises the transformation temperature to a sufficiently high $\sim$ 1250 °C.

Michael Glazoff, a scientist at the aluminum company Alcoa, informed us that there was a serious need to determine how La doping does the trick, knowledge of which might bring down the costs since lanthanum is quite expensive. It had not been possible to establish if La atoms enter the bulk, adsorb on surfaces as single atoms or clusters, or form surface compounds, but there were laboratory indications that 0.3% doping may be sufficient, whereas the industrial process seemed to require 3% doping. We resolved the puzzle as follows. Albina used a beam defocusing approach, effectively focusing the electron beam at a gradually increasing depth from the surface of an industrial La-doped γ-Al_2O_3 flake. The sequence of images in Fig. 5(a) and the line intensity plot of Fig. 5(b) clearly demonstrate that scattered single La atoms with their large atomic number Z literally light up when the electron beam is focused on the front and back surfaces but they dim considerably when the beam is defocused within the flake interior.

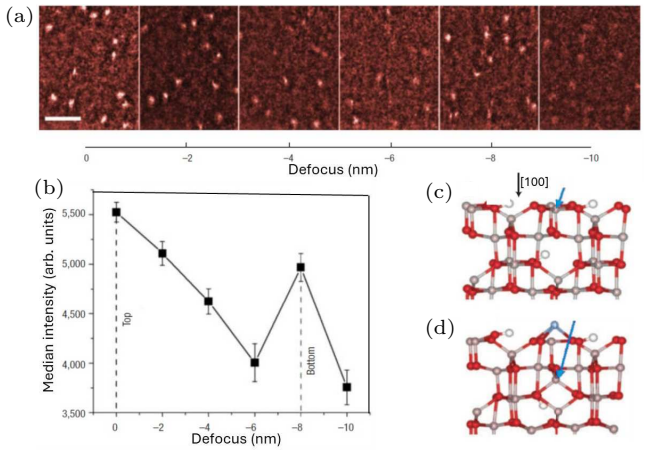


Fig. 5. La atoms on a γ-Al_2O_3 surface. (a) Z-contrast images of a La-doped γ-Al_2O_3 with the electron beam gradually focused from the top surface to the bottom surface. (b) Line plot of the median intensity as a function of depth position of the electron beam. (c) Schematic of a [100] γ-Al_2O_3 surface region (red: oxygen, gray: aluminum, white: hydrogen). (d) Configuration of a La atom on the surface. The blue arrows indicate an Al atom that is pushed by the La atom below the surface.

DFT calculations independently found that La atoms absolutely refuse to enter the interior of a γ-Al_2O_3 thin film: a La atom placed anywhere in the first few layers from the surface literally pops up to the surface; when placed anywhere deeper in the interior of the film, a La atom stays there, but its energy is much higher than when it is on the surface. On the surface, on the other hand, a La atom literally digs a hole for itself as shown in the schematics of Figs. 5(c) and 5(d): the La atom pushes a surface Al atom to a point below the surface where it bonds strongly to oxygen atoms, while it forges a strongly bonded configuration on the surface for itself. Unfortunately, by the time we drew our definitive conclusions, Alcoa had sold their catalytic aluminas division and we did not succeed in connecting with the new management to carry out industrial tests. The science stands, however.

The second example is a project for which microscopy was led by Maria.[6] Epitaxial strain often enhances or suppresses the diverse properties of complex oxides and sometimes modifies the ground state. Lanthanum cobaltite ($LaCoO_3$ or LCO) epitaxial films under tensile strain have been considered a model system for understanding the stabilization of a ground state that is not observed in bulk form:

While bulk LCO does not exhibit any long-range magnetic order, coherently strained LCO films are ferromagnetic (FM) at low temperatures. Both bulk and thin-film samples are insulating, leading to the belief that the films are stoichiometric, because any substantial deviation from stoichiometry should lead to metallic behavior; e.g., oxygen vacancies should dope the material n-type. Several theoretical studies sought to explain the insulating ferromagnetic state assuming stoichiometric films, but no consistent picture emerged. Similarly, efforts to explain the puzzle using *Z*-contrast imaging and EELS plus x-ray absorption and optical conductivity data led to the conclusion that the films are stoichiometric, as assumed by prior theoretical works, and also did not produce a viable resolution of the ferromagnetism puzzle.

The resolution of the puzzle was accomplished using extensive atomically resolved *Z*-contrast imaging of LCO films grown on a (001) $SrTiO_3$ substrate, EELS, and EELS chemical mapping of the constituent elements. These data demonstrated unambiguously that there is a significant oxygen deficiency (Fig. 6(a)). This key result anchored an intriguing theoretical resolution of the overall open puzzle. We adopted a model crystal structure with a periodic superstructure of oxygen vacancies as deduced from the data. The calculated EELS in the O-depleted and stoichiometric regions agreed with the measured spectra (Fig. 6(b)). DFT calculations found a relatively complex magnetic ordering with a net magnetic moment per Co atom equal to 1 μ_B, close to the measured values of $\sim 0.8\ \mu_B$. The pièce de résistance turned out to be the origin of the insulating state, which occurs despite the excessive oxygen-vacancy "doping" that should make the film heavily n-type (metallic). Initially, the ordered O vacancies induce Peierls minigaps at several points in the Brillouin zone (Fig. 6(c), top) [in a particular direction in the crystal, a distortion with a periodicity equal to half the Fermi wavelength ($\lambda = \pi/k_F$) opens a gap at the Fermi energy]. However, a substantial relaxation ensues, leading to a nonlinear rupture of the energy bands with a sizable energy gap (Fig. 6(c)).

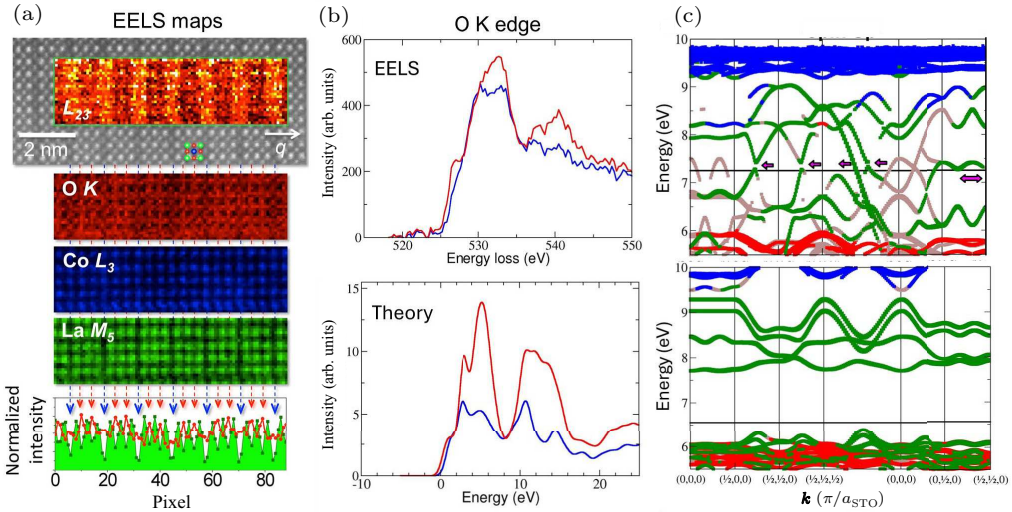


Fig. 6. Ordered oxygen vacancies in $LaCoO_3$ induce mini Peierls gaps in the initially metallic band structure; relaxation induces a rupture of the bands, turning the material into an insulator. (a) EELS-derived chemical maps indicate ordered O vacancies (dips in bottom panel of the red O *K* line spectrum are indicated by blue arrows). (b) EELS and calculated O *K* spectrum in the bulk film (red) and the O-depleted regions (blue). (c) Metallic energy bands acquire Peierls mini gaps (top) that induce relaxation and rupture of the energy bands (bottom).

4. Nanoparticles

We picked a good nanoparticle problem to test the power of combining electron microscopy and theory. Sandy Rosenthal's group at Vanderbilt was making CdSe nanoparticles with uniform diameters, down to 2 nm. They found that, when excited by 4-eV photons, the nanoparticles emit light whose color is a function of their diameter d, starting with red for $d = 6.5$ nm, through the colors of the rainbow to blue at $d = 2$ nm (Fig. 7(a)). The phenomenon is well understood in terms of quantum confinement that widens the energy gap as the diameter gets smaller. Making nanoparticles with d smaller than 2 nm proved to be quite difficult, but the expectation was that they would emit dark blue to purple light. In 2005, the group was able to produce sub-2-nm CdSe nanoparticles, but they emitted white light! That was very exciting for light applications, except for the fact that Cd is toxic and CdSe seemed to be the only nanoparticles that produced a beautiful white color.

On the science side, the origin of the white light remained a mystery. It was more than five years later that we decided to probe the question by combining electron microscopy and theory.[7] Tim Pennycook, Steve's son, had followed his father's footsteps in electron microscopy, but joined my group at Vanderbilt because he wanted to combine microscopy with theory. On the microscopy side, James McBride, Sandy's

student, joined the effort. The first hint from imaging CdSe nanoparticles was that they have a crystalline structure, but the edges get fuzzier and fuzzier as their diameter gets smaller and smaller (Fig. 7(b) left). As the diameter dips below 2 nm, crystallinity is gone and the structure seems unstable (Fig. 7(b) right). Consecutive images actually showed that the ultrasmall nanoparticles are actually quite fluxional. A video was made that demonstrated the effect. Ten frames are shown in Fig. 7(c).

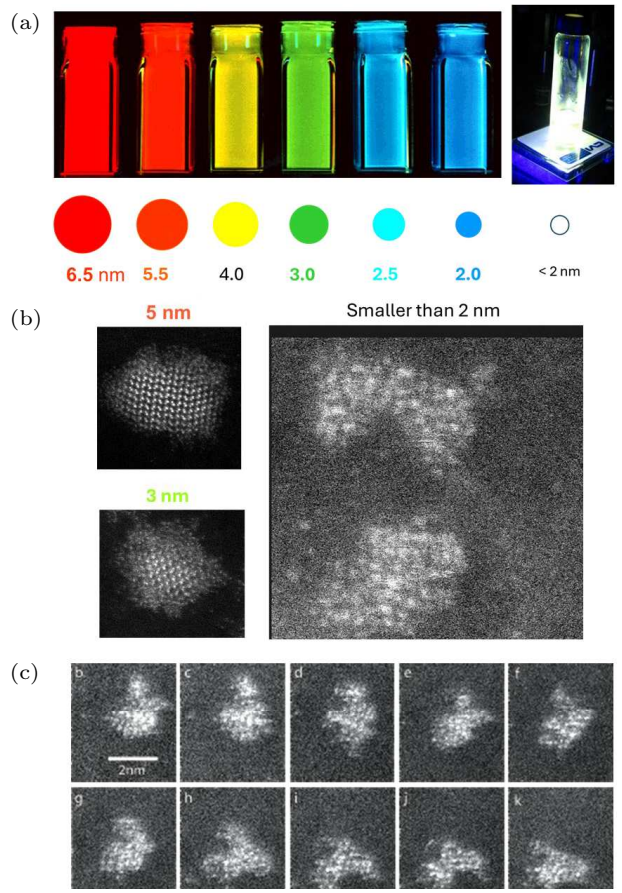


Fig. 7. Emission of light by CdSe nanoparticles of different diameters. (a) Emitted light is blue-shifted as the diameter decreases to about 2 nm. White light is emitted when the diameter dips below 2 nm. (b) Nanoparticles with diameter larger than 2 nm have a crystalline interior and fuzzy surfaces that are more extensive as the diameter decreases. Below 2 nm, the nanoparticles lose their crystallinity and are fluxional, as shown in the ten frames of a movie in panel (c).

Tim carved out an ultrasmall $Cd_{27}Se_{27}$ nanocrystal from bulk wurtzite CdSe to investigate its structural and optical properties. When he relaxed the structure using DFT, he found that the crystallinity deteriorates. He heated the structure to room temperature using DFT-based molecular dynamics (MD) and found that the cluster disorders further and the atoms move continuously. When a nanoparticle absorbs a UV photon and then emits a photon in the visible spectrum, the excess energy goes into vibrations, i.e., the nanoparticle's temperature is raised. Tim did an estimate for the temperature rise and carried out MD simulations at 500 K. He found that the nanoparticle becomes fluxional, pretty much as observed in the microscope. He then took snapshots of the nanoparticles and calculated their energy-level structure. He found that the fluxionality induces a continuous change in the energy gap, spanning the rainbow energies, from red to blue, on a time scale of 40 fs between snapshots (Fig. 8(a)). Our eyes cannot resolve colors changing so fast so that the whole spectrum gets blended into white light. A simulated spectrum of the intensities of emitted photon energies that together appear as white light matches the measured spectrum (Fig. 8(b)). The origin of white light is explained.

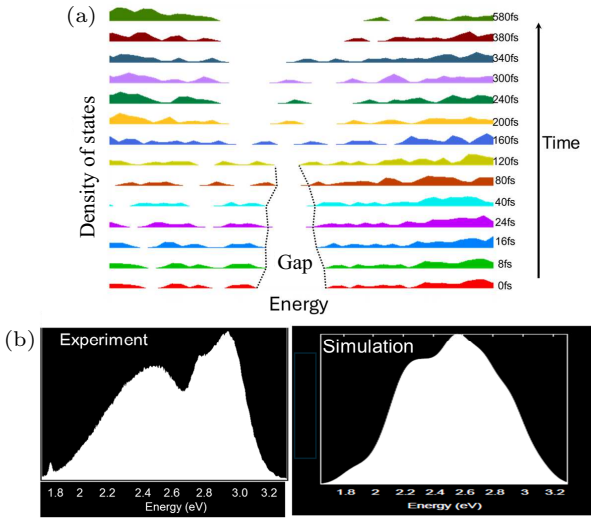


Fig. 8. Calculated density of states (DOS) of a nanoparticle with diameter smaller than 2 nm and emitted white-light spectrum from experiment and simulation. (a) The gap between occupied and empty states changes in magnitude as the nanoparticle becomes fluxional when it absorbs a 4-eV photon. The DOS color corresponds to the emitted light according to the value of the gap. Our eyes cannot resolve the colors on the fast time scale on the right vertical axis. (b) Measured and simulated white-light spectra.

5. Two-dimensional materials and nanowires

Of course we paid attention to 2D materials, beginning with the emergence of graphene as a miracle material. I will describe what became a multigenerational effort using just a few examples. Juan Carlos Idrobo had joined the ORNL group as a post-doc with the intention to do both microscopy and theory. He was good at doing theory, but he gradually gravitated to full-time microscopy and became a staff member. He succeeded in getting a National Science Foundation grant through his Vanderbilt post-doc appointment and in 2010 hired Wu Zhou, a fresh-Ph.D. microscopist from Lehigh University. In 2012, Wu was awarded a two-year Wigner Fellowship which led to a staff position. That's three generations of microscopists (there is more to come). We worked on quite a few problems. Here are a couple of them.

The first project was anchored on a Si_6 cluster that was found by Wu embedded in a graphene nanopore.[8] In different images of the cluster, one of the Si atoms was found in one of two different positions. A movie was made and the Si atom was indeed seen to jump back and forth (eight frames from the

movie can be seen in Fig. 9(a)). DFT calculations determined the energy barrier for this transformation to be 1.44 eV from the ground state to the metastable state and only 0.8 eV for the reverse jump. These numbers allowed us to estimate that the rates of thermal forward and reverse jumps would differ by more than ten orders of magnitude, whereas the measured rates differ by only a factor of two. The electron scattering rates for the two jumps were calculated and found to differ by roughly a factor two, confirming that the observed jumps are induced by the electron beam. This finding was the first observation of an electron-beam-induced reversible conformational transformation of an embedded cluster. Finally, DFT calculations further demonstrated that, though the Si cluster is bonded to the surrounding graphene, it maintains very close similarity to a free six-atom Si cluster.

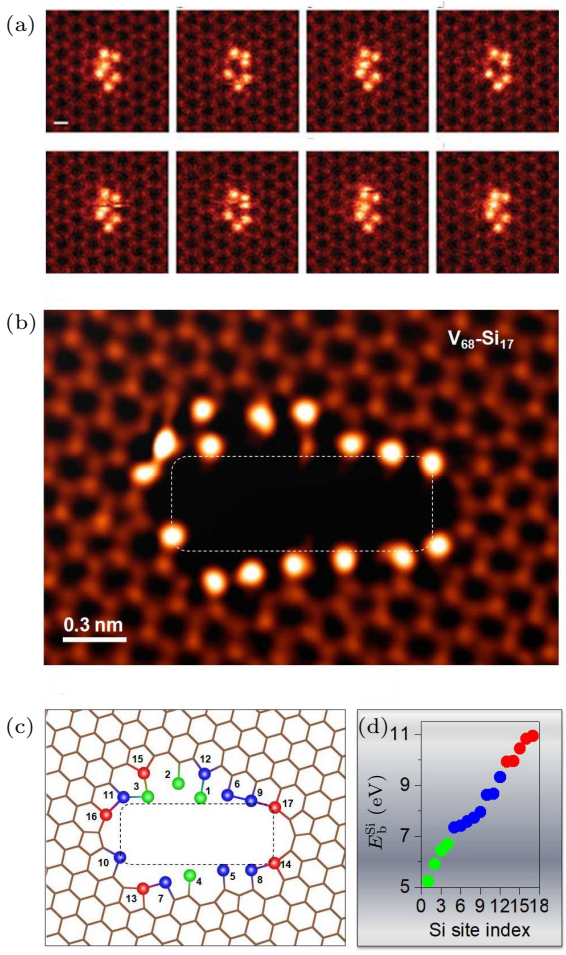


Fig. 9. Structures in graphene. (a) *Z*-contrast images of a six-silicon-atom cluster embedded in a graphene nanopore. The eight panels are frames from a movie showing jumps of one of Si atoms from left to right (reversible, beam-induced transformation). (b) A fairly large pore in graphene passivated by Si atoms. (c) DFT calculations find that the Si bonds to the graphene C atoms are very strong, as shown in panel (d).

In a related project,[9] a fairly large nanopore was found in a graphene sample, featuring passivation of the rim by Si atoms (Fig. 9(b)). The nanopore was stable over days, indicating a very robust passivation. DFT calculations indeed found very large Si–C bonding energies, ranging from 5 eV to 11 eV (Figs. 9(c) and 9(d)). Unpassivated nanopores in graphene are known to fill relatively quickly because there are always excess C atoms and hydrocarbons around. DFT calculations also found that hydrogen atoms are not good passivators of nanopores in graphene, leading to the conclusion that Si atoms would be the best choice. Systematic studies of passivated multivacancies demonstrated the possibilities of engineering stable nanopores for applications. We got very excited about the prospects and filed a patent disclosure at Vanderbilt. The Vanderbilt patent office liked the prospects of a possible patent, but they were careful to test the market before actually going through the expensive patent-application process. They found a company that would like to have samples with passivated nanopores to test applications. Our microscopy/theory group, however, once more, did not have the expertise and mission to get into fabrication so the project was dropped.

At about the same, I had a new graduate student, Junhao Lin, intending to pursue a joint microscopy/theory thesis. He had finished his coursework and theoretical training at Vanderbilt and moved to ORNL to do the microscopy part of his thesis. Wu became his mentor — four generations of microscopists at the same place: Pennycook–Idrobo–Zhou–Lin! Junhao was prolific. One of his accomplishments was to use the electron beam to fabricate nanowires in MoS_2 and $MoSe_2$ monolayers and image the process at the same time, making movies that can be seen in the supplementary material of Ref. [10]. The first panel of Fig. 10(a) shows a Y-junction that Junhao patiently sculpted and imaged in a MoS_2 monolayer. The remaining panels show a sequence of images taken during the sculpting of a nanowire in $MoSe_2$, with the clock set at $t = 0$ s in the first panel; the clock time of the subsequent panels is shown at the top each panel. Something unusual happened: It took 350 s, almost 6 minutes to sculpt the nanowire shown in the second panel; initiation of further thinning, as seen in the third panel, took 43 more seconds, but, suddenly, the outer atomic layer peeled off spontaneously in only a few seconds, leaving a beautiful three-atom-thick nanowire. Junhao constructed a structural model of the nanowire connected to the monolayer, demonstrated that the contact is Ohmic, and calculated projected densities of states to show that the energy gap of $MoSe_2$ quickly goes to zero within the nanowire, suggesting metallic behavior (Figs. 10(b)–10(d)) — a thrilling prospect of being able to fabricate three-atom conducting nanowires to interconnect devices that other groups had already fabricated on monolayers. The ORNL microscopes at the time did not have the capability of *in-situ* electrical measurements. A connection was established with Kazu Suenaga in Tokyo who had such a capability and the conducting nature of the three-atom-thick nanowires was confirmed. Upon graduation, Junhao was awarded a coveted post-doctoral fellowship by the Japan Society for the Promotion of Science and joined Suenaga's group for a very fruitful career start.

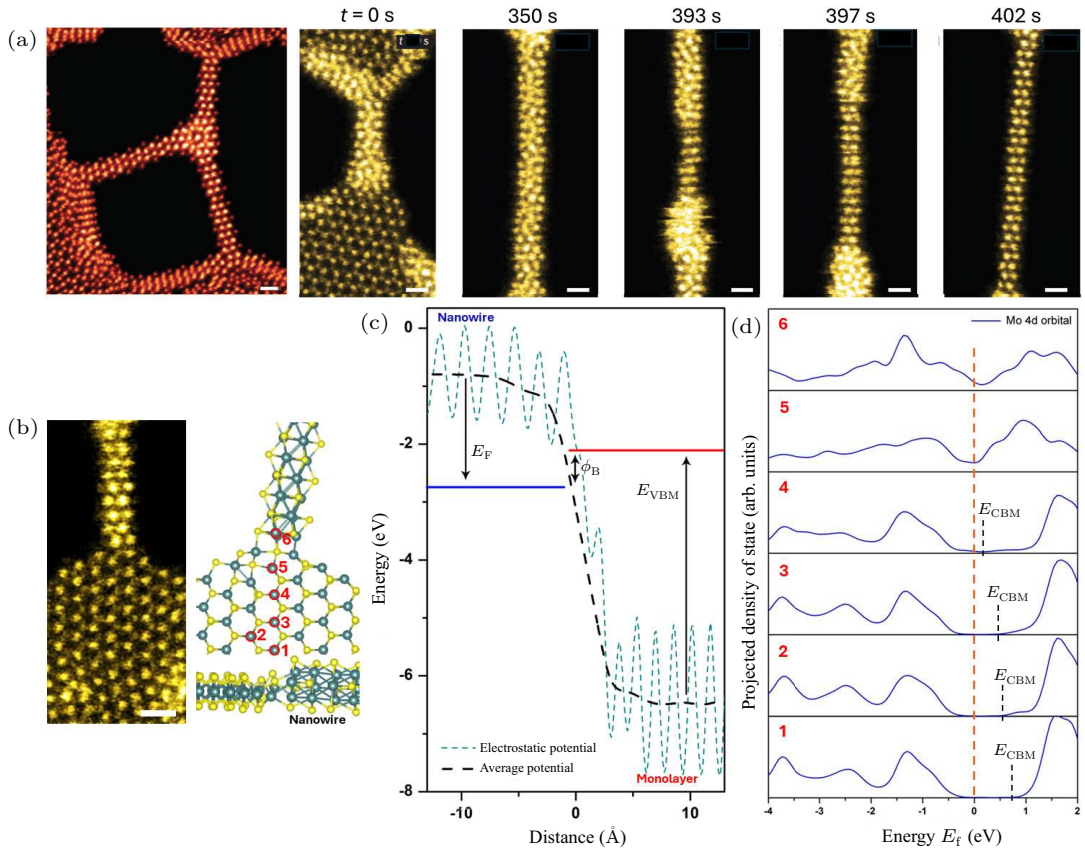


Fig. 10. Nanowires fabricated in monolayer MoS_2 and $MoSe_2$. (a) Left panel: Y junction in MoS_2. Right five panels: sequence of sculpting a nanowire in $MoSe_2$. The sculpting is initially relatively slow, but in the last three frames a very fast spontaneous thinning to three atoms across occurs. (b) Junction of the nanowire to the monolayer $MoSe_2$ and schematic of the atom structure. (c) Calculated electrostatic potential and band alignment showing an Ohmic contact. (d) Calculated projected densities of states at the sites indicated by numbers in the schematic of panel (b), demonstrating that at sites 5 and 6 the nanowire displays metallic behavior.

6. Summary, recent developments, and the future

The above examples illustrate the high degree of complementarity between STEM/EELS experiments and DFT calculations in a variety of contexts, materials, and nanostructures. Long standing issues can be resolved and deep insights can be gained in the mechanisms that underlie observations. In many cases, ways had to be found to overcome practical limits of current computers. In other cases, calculations probed where experiments were not (yet) able to go. Predictions were made that could in principle be tested at a later time.

The journey that I started with Steve has continued with former members of his group, including several of my own former students, a very rich turf overall. In fact, I currently have a student at ORNL, Harrison Walker, mentored by my former student, currently staff microscopist, Jordan Hachtel. Jordan's post-doc Eric Hoglund is co-mentoring. The group leader is now long-time group member Andy Lupini — multigenerations again at work. Following the revolution in achieving sub-Ångstrom spatial resolution for both imaging and EELS with aberration-corrected STEM, spearheaded by Ondrej Krivanek and his team at Nion, Inc., during the two decades I worked with Steve, the STEM/EELS field has undergone significant enrichment in the last decade with new instrumentation. I am not in the know of all major instrumental developments, but I will mention just a few, for which DFT calculations are meeting the new challenges.

Yuichi Ikuhara, Naoya Shibata (a former visitor in Steve's group at ORNL), and their team at the University of Tokyo pioneered differential phase contrast STEM (DPC STEM) that enables atomic-resolution mapping of electric fields, from which one gets the charge density by Gauss's law, and magnetic fields. It was a privilege to work with ORNL microscopists Miaofang Chi, Jordan Hachtel, and Juan Carlos Idrobo to analyze charge distributions obtained for the first time in an electride, Y_5Si_3, which hosts anionic electrons in interstitial columns.[11] There was a surprise: inhomogeneities in some of the anionic-electron columns. DFT calculations of the electron distribution and comparisons with the data made a strong case that the inhomogeneities originate from hydrogen traces. The presence of hydrogen in the material was corroborated by neutron scattering. Such hydrogen trace concentrations, undetectable by other means, can impact the many properties that anionic electrons are known for.

In situ experiments in STEM, such as the application of voltages on samples, heating and cooling of samples

("cryo STEM"), shining light on samples, etc. are becoming widespread. DFT calculations are ready to play. In recently published work with my former student Junhao Lin, who was mentioned earlier in this perspective, Junhao and his students at the Southern University of Science and Technology in Shenzhen, China, applied a voltage to $MoTe_2$ films sandwiched between graphite sheets, produced highly oriented Mo_6Te_6 nanowires, and imaged the dynamics.[12] DFT calculations and broader theoretical considerations helped account for the dynamics of the process. Cryogenic STEM is of course here and has enormous promise as the technology to achieve and maintain low temperatures is improving rapidly. We in fact have joint work on high-temperature STEM/EELS with the Nion team and Idrobo (now at the University of Washington), as well as cryo-STEM with Hachtel, both to be published soon.

Perhaps the most consequential advancement in STEM/EELS in the last decade is the advent of a new generation of monochromators, also spearheaded by Krivanek and his Nion team, that results in unprecedented EELS energy resolution, with the current record being 2.4 meV. Previously the energy resolution was of order 1 eV, which meant that phonon and, more generally, vibrational spectra were not accessible. The new monochromators opened new frontiers and led to an explosion of work on vibrational spectroscopy with atomic-scale resolution so that the phonons at defects can be mapped out and on measurements of phonon-polariton dispersions. DFT calculations again are instrumental in documenting and analyzing the measured spectra. Our own work in the context of vibrational EELS with Jordan Hachtel[13–15] and with Wu Zhou,[16] now at the University of the Chinese Academy of Sciences in Beijing, China, complements work by others and has led to fascinating new insights in emergent phonons in superlattices,[13] in localized phonons at grain boundaries,[14] in phonon spectra with chemical-bond sensitivity,[15] and a tantalizing theoretical discovery that lattice vibrations form vortices around heavy impurities such as Si in graphene and P and Al in monolayer hexagonal BN.[17] Even more recently, we reported on the nonequivalence of AlN–$(Al_{0.65}Ga_{0.35})$N and $(Al_{0.65}Ga_{0.35})$N–AlN interface vibrations in AlN–$Al_{0.65}Ga_{0.35}$ superlattices, with Eric and Harrison as first-coauthors.[18] The tradition of joint theory/experiment Ph.D. theses that started during Steve's tenure at ORNL still marches on!

Vibrational EELS at different temperatures, from cryo to very high temperatures, either spatially resolved or momentum resolved, or even at hybrid resolution between the two, is bringing another form of DFT calculations to the forefront of developments in the STEM universe, namely, DFT-based "molecular dynamics" (MD) simulations. This archaic terminology shortchanges the power of the technique as it applies to any statistical ensemble of atoms such as crystals, heterostructures, superlattices, and of course liquids made up of molecules such as water. Atoms are allowed to move according to Newton laws under whatever quantum forces are exerted by all the other atoms as calculated by ground-state DFT. By simulating the equilibrated evolution of a canonical ensemble over tens of picoseconds at a chosen temperature, one can deduce vibrational densities of states and other quantities of interest at that temperature. The recent advent of machine-learning potentials, deep learning, and artificial intelligence, which has advanced considerably in recent years is nowadays fomenting a new revolution in vibrational spectroscopies. By running diverse DFT-based MD simulations, say at different temperatures, one has a huge number of snapshots. By "training" machine-learning potentials (MLPs) to reproduce DFT-calculated total energies and forces in the totality of snapshots, one can produce and test MLPs that play the role of "classical potentials" in MD simulations. Such DFT-trained and validated MLPs can then be used in MD simulations to extract vibrational properties for very large systems, breaking the severe computer-performance-imposed limitations on the number of atoms that can be handled by straight DFT simulations. Hundreds of thousands, even millions of atoms can be handled using MLPs. MLPs have already been used to calculate lattice thermal conductivities by several investigators and only recently are making their appearance in vibrational properties. We have had an initial entry in the field[19] and have completed projects that are still to be published plus work in progress. The future is here!

One final recent development is notable advances in EELS simulations, including vibrational EELS by several groups (e.g., Zeiger and Rusz as in Ref. [20] and D. J. Masiello's group as in Ref. [21] and other papers). Such simulations go beyond analyzing vibrational EELS by comparing with vibrational densities of states, which has worked well in the pioneering work of recent years. These more advanced simulations include realistic scattering of the beam electrons from the system vibrations at different momentum transfers, the impact of the vibrations on the electron beam as it travels to the detector, the dynamical diffraction that the beam undergoes as it traverses layers of atoms in the system, and more. At their core, they need good calculations of the vibrational/phonon modes at whatever temperatures EELS is performed. The latter is challenging, but they are doable. The impact of the new EELS simulators on analyzing vibrational EELS is forthcoming.

STEM and STEM/EELS, the several variants mentioned above and many more variants that have not been mentioned are continually opening new frontiers. Steve can be very proud of his pioneering work, the many innovations that he fostered, the countless microscopists that he mentored, and his scien-

tific accomplishments. I am proud to have been a participant in that extraordinary journey.

Acknowledgments

All of my work relating to STEM/EELS at ORNL and at Vanderbilt University over the years has been funded by the U.S. Department of Energy, Office of Science, Materials Science and Engineering Division. All figures in this paper are adapted from figures in the cited papers.

References

[1] Maiti A, Chisholm M F, Pennycook S J and Pantelides S T 1996 *Phys. Rev. Lett.* **77** 1306
[2] Chisholm M F, Maiti A, Pennycook S J and Pantelides S T 1998 *Phys. Rev. Lett.* **81** 132
[3] Yan Y, Chisholm M F, Duscher G, Maiti A, Pennycook S J and Pantelides S T 1998 *Phys. Rev. Lett.* **81** 3675
[4] Klie R, Buban J P, Varela M, Franceschetti A, Jooss C, Zhu Y, Browning N D, Pantelides S T and Pennycook S J 2005 *Nature* **435** 475
[5] Wang S, Borisevich A Y, Rashkeev S N, Glazoff M V, Sohlberg K, Pennycook S J and Pantelides S T 2004 *Nat. Mater.* **3** 143
[6] Biškup N, Salafranca J, Mehta V, Oxley M P, Suzuki Y, Pennycook S J, Pantelides S T and Varela M 2014 *Phys. Rev. Lett.* **112** 087202
[7] Pennycook T J, McBride J R, Rosenthal S J, Pennycook S J and Pantelides S T 2012 *Nano Lett.* **12** 3038
[8] Lee J, Zhou W, Pennycook S J, Idrobo J C and Pantelides S T 2013 *Nat. Commun.* **4** 1650
[9] Lee J, Yang Z, Zhou W, Pennycook S J, Pantelides S T and Chisholm M F 2014 *Proc. Natl. Acad. Sci. USA* **111** 7522
[10] Lin J, Cretu O, Zhou W, Suenaga K, Prasai D, Bolotin K I, Cuong N T, Otani M, Okada S, Lupini A R, Idrobo J C, Caudel D, Burger A, Ghimire N J, Yan J, Mandrus D G, Pennycook S J and Pantelides S T 2014 *Nat. Nanotechnol.* **9** 436
[11] Zheng Q, Feng T, Hachtel J A, Ishikawa R, Cheng Y, Daemen L, Xing J, Idrobo J C, Yan J, Shibata N, Ikuhara Y, Sales B C, Pantelides S T and Chi M 2021 *Sci. Adv.* **7** eabe6819
[12] Yang Q, Wang Y P, Shi X L, Li X X, Zhao E, Chen Z G, Zou J, Leng K, Cai Y, Zhu L, Pantelides S T and Lin J 2024 *Nat. Commun.* **15** 6074
[13] Hoglund E R, Bao D L, O'Hara A, Makarem S, Piontkowski Z T, Matson J R, Yadav A K, Haislmaier R C, Engel-Herbert R, Ihlefeld J F, Ravichandran J, Ramesh R, Caldwell J D, Beechem T E, Tomlo J A, Hachtel J A, Pantelides S T, Hopkins P E and Howe J M 2022 *Nature* **601** 556
[14] Hoglund E, Bao D L, O'Hara A, Pfeifer T, Hoque Md S B, Makarem S, Howe J M, Pantelides S T, Hopkins P E and Hatchel J A 2023 *Adv. Mater.* **35** 2208920
[15] Hoglund E R, Walker H A, Hussain M K, Bao D L, Ni H, Mamun A, Baxter J, Caldwell J D, Khan A, Pantelides S T, Hopkins P E and Hachtel J A 2024 *Adv. Mater.* **36** 2402925
[16] Xu M, Bao D L, Li A, Gao M, Meng D, Li A, Du S, Su G, Pennycook S J, Pantelides S T and Zhou W 2023 *Nat. Mater.* **22** 612
[17] Bao D L, Xu M, Li A W, Su G, Zhou W and Pantelides S T 2024 *Nanosc. Horiz.* **9** 248
[18] Hoglund E R, Walker H A, Hussain Md K, Bao D L, Ni H, Mamun A, Baxter J, Caldwell J D, Khan A, Pantelides S T, Hopkins P E and Hachtel J A 2024 *Adv. Mater.* **36** 2402925
[19] Walker H A, Hoglund E R, Bao D L, Hussain Md K, Ni H, Mamun A, Baxter J, Khan A, Caldwell J D, Hopkins P E, Hachtel J A and Pantelides S T 2024 *Microsc. Microanal.* **30** 455
[20] Zeiger P M and Rusz J 2020 *Phys. Rev. Lett.* **124** 025501
[21] Rossi A W, Bourgeois M R, Walton C and Masiello D J 2024 *Nano Lett.* **24** 7748